Magnetotransport and photoluminescence of two-dimensional hole gases in $Si/Si_{1-x}Ge_x/Si$ heterostructures

R. Loo, L. Vescan, A. Hartmann, R. Apetz, U. Zastrow, T. Schäpers, A. Leuther, C. Dieker, and H. Lüth
Institut für Schicht- und Ionentechnik (ISI), Forschungszentrum Jülich GmbH, D-52425 Jülich, Germany

P. Gartner and T. Stoica
Institute of Physics and Technology of Materials, Bucharest, MG7, Romania

(Received 26 July 1994)

The electrical and optical properties of $Si/Si_{0.8}Ge_{0.2}/Si$ p-type modulation-doped heterostructures grown on (001) Si using low-pressure chemical-vapor deposition are investigated by a variety of techniques. The thickness of the $Si_{1-x}Ge_x$ quantum well was about 15 nm and the modulation-doping effect has been obtained by two remote boron-doped ~10-nm-thick Si layers. We found a mobility enhancement at low temperatures in all modulation-doped heterostructures. Clear Shubnikov–de Haas oscillations and quantum Hall plateaus confirm the presence of a two-dimensional hole gas. From the Hall-effect measurements a hole mobility of 6870 $cm^2/V\,s$ at a sheet-hole concentration of 4.5×10^{11} cm^{-2} at 50 mK was obtained, which is comparable with the best published values for $x=0.2$. The experimental results were compared with self-consistent calculations of the valence-band diagram and hole concentration. The values for the effective mass used for the calculations were obtained by solving the 6×6 Luttinger-Kohn Hamiltonian. The photoluminescence from the $Si_{1-x}Ge_x$ quantum well shows excitonic behavior according to its variation with excitation power. A general trend of increasing photoluminescence intensity with the mobility of the two-dimensional hole gas was observed. The high hole mobility and strong photoluminescence reflect the good interfacial quality of the $Si/Si_{1-x}Ge_x/Si$ heterointerfaces grown by low-pressure chemical-vapor deposition.

I. INTRODUCTION

In the last few years the $Si_{1-x}Ge_x/Si$ system has raised considerable interest because of its successful application in silicon-based circuits.[1] In particular, two-dimensional hole gases (2DHG) play the key role in the p-channel modulation-doped field-effect transistor (MODFET), and for this reason, many groups are involved in this research.

The first detailed investigation of modulation p-doped $Si/Si_{1-x}Ge_x$ heterostructures was done by People *et al.*[2] on layers grown by molecular beam epitaxy (MBE). They studied the effects of spacer thickness, alloy layer thickness, and supply layer doping concentration on the hole mobility of modulation-doped $Si/Si_{0.8}Ge_{0.2}$ heterostructures. They reached a peak 2D hole mobility of 3300 $cm^2/V\,s$ at 4.2 K at a sheet charge density of 6.2×10^{11} cm^{-2} and from the temperature dependence of the Shubnikov-de Haas envelope function, a hole effective mass of $m_h^*=(0.32\pm0.03)m_0$ resulted. Nützel *et al.*[3] observed an increase of mobility under illumination of the heterostructure. Hole mobilities up to 4300 $cm^2/V\,s$ at a carrier concentration of 3×10^{11} cm^{-2} at 1.5 K were found for a 40-nm-thick $Si_{0.77}Ge_{0.23}$ quantum well (QW) grown by MBE. Smith *et al.*[4] reported for MBE grown layers (with $x=0.2$), a hole mobility of $\mu=3640$ $cm^2/V\,s$ (sheet hole concentration of 2×10^{11} cm^{-2} at 5.4 K) supposed to be limited by scattering on charged interface states. To the knowledge of the authors, the highest hole mobility in $Si_{0.8}Ge_{0.2}$ channels grown by MBE was measured by Mishima *et al.*[5] ($\mu=6000$ $cm^2/V\,s$ with $p=1\times10^{12}$ cm^{-2} at 2 K). The single-doped heterostructures with the doped layer on the surface side revealed a higher mobility than the inverted structure (doped layer on the substrate side). The difference in the measured mobility was attributed to surface segregation of boron.

An ultrahigh-vacuum chemical-vapor deposition (UHV-CVD) system was used by Fang *et al.*[6] to grow modulation-doped structures. They investigated both single-side-doped and symmetrically doped heterostructures and measured hole mobilities in the range of 5000–7000 $cm^2/V\,s$ at 1.4 K. They found two 2DHG's in the symmetrically doped samples which consisted of a 40-nm-thick $Si_{1-x}Ge_x$ layer with a Ge mole fraction of 10–12 %. The $Si_{1-x}Ge_x$ layer was thick enough for the development of 2DHG's at both interfaces. The measured hole density in the QW was $(3.7-12)\times10^{11}$ cm^{-2}. Venkataraman, Schwartz, and Sturm[7] ($\mu_h=2500$ $cm^2/V\,s$ and $p=6\times10^{11}$ cm^{-2} at 10 K with $x=0.15$) and Guldner *et al.*[8] ($\mu_h=4000$ $cm^2/V\,s$ and $p=6.2\times10^{11}$ cm^{-2} at $T\approx1.5$ K with $x=0.2$) studied single-doped and symmetrically doped layers grown by rapid thermal chemical-vapor deposition (RTCVD). Investigations on modulation-doped $Si/Si_{0.8}Ge_{0.2}$ heterostructures grown by a low-pressure chemical-vapor deposition (LPCVD) were done by Vescan *et al.*[9] and Apetz *et al.*[10] ($\mu_h=6870$ $cm^2/V\,s$, $p=4.5\times10^{11}$ cm^{-2} at 50 mK).

Nayak *et al.*[11] have studied the feasibility of a p-channel quantum-well metal-oxide-semiconductor field-effect transistor (MOSFET) on a $Si_{1-x}Ge_x/Si$ heterostructure grown by molecular-beam epitaxy (MBE). They found an increase of the 300-K channel mobility

($\mu_h = 155$ cm^2/V s) for a $Si_{0.8}Ge_{0.2}$ channel as compared to $\mu_h = 120$ cm^2/V s for a Si channel with the same layer structure. Kesan *et al.*[12] have grown similar structures by UHV-CVD and found an increase of the mobility from 95 cm^2/Vs (Si) to 150 cm^2/V s ($Si_{0.8}Ge_{0.2}$) at 300 K and from 250 cm^2/Vs (Si) to 400 cm^2/V s at 82 K. In these studies the mobility is extracted from the slope of the saturation transconductance versus gate voltage curve for a long channel device [10 μm (Ref. 11) and 1.85 μm (Ref. 12), respectively]. Similar investigations were performed by Garone, Venkataraman, and Sturm[13] using RTCVD, while Verdonckt-Vandebroek *et al.* grew layers by UHV-CVD using a graded $Si_{1-x}Ge_x$ channel.[14] A *p*-type modulation-doped field-effect transistor (MODFET) grown by MBE was investigated by Pearsall and Bean.[15]

In this paper we present investigations of modulation-doped Si/$Si_{0.8}Ge_{0.2}$/Si double heterostructures grown by low-pressure chemical-vapor deposition. Besides the results of magnetotransport measurements, we compare transmission-electron microscopy (TEM) micrographs with depth profiles obtained by secondary-ion mass spectrometry (SIMS) and electrochemical capacitance voltage (eCV). We performed effective-mass and self-consistent valence-band calculations. Finally we present the results of photoluminescence (PL) measurements on modulation-doped $Si_{1-x}Ge_x$/Si heterostructures. We report the observation of strong PL from modulation-doped Si/$Si_{1-x}Ge_x$/Si structures and discuss the origin of the different peaks. An interesting property is the enhancement of the PL intensity from the modulation-doped $Si_{1-x}Ge_x$ QW relative to undoped QW structures. A possible explanation of this effect is given.

II. LPCVD GROWTH AND LAYER SEQUENCE

The Si/$Si_{1-x}Ge_x$/Si layers investigated in this work were deposited by selective epitaxial growth using a load-locked low-pressure chemical-vapor deposition system. Details of this growth technique have been described elsewhere.[16] The substrates were lightly doped (10^{13} cm^{-3}) *n*-type (001) Si wafers for electrical, SIMS, and PL measurements and moderately doped (10^{15} cm^{-3}) *p*-type (001) wafers for SIMS, TEM, and eCV measurements. Wafers with oxide patterns for in-filling selective growth were loaded into the reactor after a RCA cleaning and a HF dip. The sample area was 8×8 mm^2. Figure 1 shows the temperature during the growth of the modulation-doped samples. The epitaxy was performed at 680–800 °C for the Si layers, and at 680 °C for the $Si_{0.8}Ge_{0.2}$ layers. The pressure in the reactor during epitaxy was 0.12 torr and the gases used are $SiCl_2H_2$, GeH_4, H_2 (carrier gas), and as doping gas B_2H_6 (20 ppm in H_2).

The samples have the following layer sequence (see also Fig. 1 and Table I). First, a 100–300-nm undoped Si buffer layer was grown. Subsequently, a 12-nm-thick boron-doped [$(3-11)\times10^{18}$ cm^{-3}] layer, a Si spacer layer (9–37 nm), a 15-nm-thick $Si_{0.8}Ge_{0.2}$ layer with $x\sim0.2$, a second Si spacer (9–37 nm), a second boron-doped [$(3-11)\times10^{18}$ cm^{-3}] layer, and an undoped Si cap layer (20–65 nm) were grown. The $Si_{0.8}Ge_{0.2}$ layer was made sufficiently thin so that only one 2DHG channel should be formed. The $Si_{0.8}Ge_{0.2}$ layer thickness was much lower than the critical thickness associated with strain relaxation by nucleation of misfit dislocations on a large area ($\sim$75 nm).[17] Therefore the $Si_{0.8}Ge_{0.2}$ layer should be pseudomorphic. Homogeneously doped Si layers with different doping levels were grown in order to calibrate the incorporated concentration of boron atoms with the B_2H_6 flow rate. A specimen (sample 476) with the same doping sequence as the modulation-doped heterostructure but without the $Si_{0.8}Ge_{0.2}$ layer was grown in order to study the electrical properties of the thin boron-doped Si layers. A uniformly doped (1×10^{18} cm^{-3}) Si/$Si_{0.8}Ge_{0.2}$/Si structure (sample 475) was also grown. Table I contains a list of the investigated samples.

Layer thicknesses and Ge compositions in the heterostructures were obtained by Rutherford backscattering spectroscopy (RBS) and SIMS. TEM was performed with a JEOL 4000FX electron microscope at 400 kV on (001) plan-view and {110} cross-section specimens prepared by Ar^+ ion milling. SIMS depth profiling was performed in a quadrupole instrument (a modified ATOMIKA ADIDA 3000-30) with an O_2^+ primary beam at 2° with respect to the sample normal and a

TABLE I. List of samples investigated in this study.

Sample no.	Basic structure	Spacer width (nm) SIMS	Well width (nm) SIMS	Well width (nm) RBS	Ge content RBS
459	Si, homog. doped				
436	Si, homog. doped				
437	Si, homog. doped				
438	Si, homog. doped				
476	Si, two 10-nm doped layers				
475	Si/$Si_{1-x}Ge_x$/Si, homog. doped		12	12	0.2
479	Si/$Si_{1-x}Ge_x$/Si, mod. doped	9	11	15	0.2
478	Si/$Si_{1-x}Ge_x$/Si, mod. doped	10	13	16	0.2
509	Si/$Si_{1-x}Ge_x$/Si, mod. doped	10	12	12	0.13
464	Si/$Si_{1-x}Ge_x$/Si, mod. doped	16	15	18	0.2
534	Si/$Si_{1-x}Ge_x$/Si, mod. doped	36	13	17	0.2
535	Si/$Si_{1-x}Ge_x$/Si, mod. doped	37	16	19	0.2

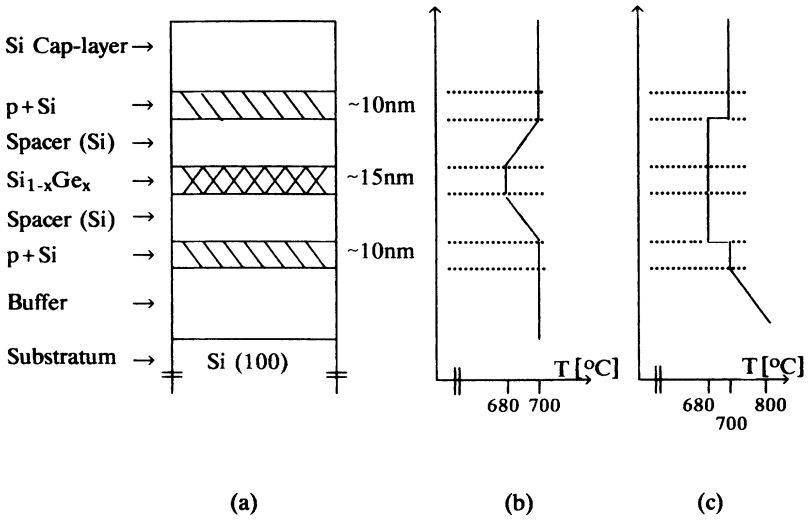

FIG. 1. Schematic of the modulation-doped samples investigated in this paper. (a) Layer sequence, (b) growth temperature of the samples 464, 478, 479, and 509, and (c) growth temperature of the samples 534 and 535.

primary-ion energy of 1.5–12 keV. Further characterization details of the SIMS measurements are given in Ref. 18. For the electrochemical CV measurements we used a polaron profile plotter (PN4300) with a NH_4F-HF-based electrolyte. A detailed description of the electrochemical CV method is given in Refs. 19 and 20. The electrical properties were determined between 4 and 300 K by conventional Hall-effect–van der Pauw measurements with a magnetic field of $B=0.50$ T. Shubnikov–de Haas (SdH) and quantum-Hall-effect (QHE) measurements were performed at $T=50$ mK. For these measurements a Hall-bar geometry was used. For the Ohmic contacts the following metal sequence was evaporated: Al(20 nm)/Ti(20 nm)/Au(100 nm)/Cr(50 nm) and alloyed at 380 °C for 5 min. PL was carried out with a Fourier transform spectrometer equipped with a N_2-cooled Ge detector. The samples were mounted in a continuous-flow He cryostat and excited by an Ar ion laser (488 nm).

III. DEPTH PROFILES

Figure 2(a) shows a TEM micrograph of a modulation-doped $Si/Si_{0.8}Ge_{0.2}/Si$ double heterostructure (sample 534) with symmetric doping. The $Si_{0.8}Ge_{0.2}$ layer is clearly observed as a dark stripe. The TEM micrograph shows a high degree of perfection of the $Si_{0.8}Ge_{0.2}$ layer characterized by homogeneous thickness and planar interfaces. No misfit dislocations are seen. However, PL measurements show D_1 (0.812 eV) and D_2 (0.875 eV) lines characteristic for misfit dislocations.[21] The peak intensities are very low, but nevertheless the presence of D_1 and D_2 lines indicates that there are some dislocations at the $Si/Si_{0.8}Ge_{0.2}$ interface (on the substrate side), whose density is low enough so that they could not be detected in TEM pictures.

In Fig. 2(b) the SIMS and eCV depth profiles of sample 534 are plotted. The boron-doped regions and the $Si_{1-x}Ge_x$ layer are given by SIMS. While the eCV measurement shows only the electrically active dopant concentration, SIMS detects all dopant atoms. Several authors have discussed CV measurements of narrow doped layers buried within a thick semiconductor layer.[22–24] They showed that, in a narrow boron-doped layer, holes will diffuse out to both sides, leaving a negative space charge which generates the drift field necessary to balance hole diffusion for stationary conditions. Therefore the measured hole density in the center of the doped layer is lower than the total boron concentration. Furthermore, due to the Schottky contact between the electrochemical solution and the sample, some holes of the boron-doped layer on the surface side are removed out of the surface depletion layer. In our eCV measurements we get a depth profile by alternating CV measurements and etch steps. Therefore, holes which are removed by the Schottky contact before the first CV measurement was made are not detected. The etch steps (10 nm) certainly have some effect on the depth resolution due to the surface roughness of the etch crater, leading to an error in eCV depth measurements of 15%.

The depths of the boron-doped supply layers (57 and 141 nm) obtained by SIMS [Fig. 2(b)] are in good agreement with the eCV measurement (63 and 134 nm). In agreement with the above discussion, the measured hole concentration peak of the doped layers (eCV) is lower than the boron concentration peaks (SIMS). Furthermore, following the results from literature[22,23] we compare here sheet concentrations instead of volume concentrations. So, from the SIMS we get values of $N_A=(6.0\pm1.2)\times10^{12}$ cm^{-2} for the surface side layer and $N_A=(4.9\pm1.0)\times10^{12}$ cm^{-2} for the substrate side layer. Comparing these values with the hole concentration from eCV [$p=(2.0\pm0.4)\times10^{12}$ cm^{-2} and $p=(4.7\pm0.9)\times10^{12}$ cm^{-2}, respectively], we see that the hole density on the surface side is lower than the boron concentration. This must be due to outdiffusion of holes, as discussed above. Together with the result of the Hall-effect measurement, which gives the hole concentration of both boron-doped layers [$p_{300\,K}=(1.6\pm0.1)\times10^{13}$ cm^{-2}], we can conclude that boron is fully activated.

It is striking that the spacer widths in the SIMS profile are not equal, i.e., the surface side spacer is thicker. Therefore, the SIMS depth profiling of $Si/Si_{1-x}Ge_x$ het-

erostructures was studied in detail and it was found that Ge accumulates at the back side of the sputtering-induced oxide layer.[18] The delayered transport of Ge through the oxide layer leads to an increasing shift of Ge to greater depth with rising primary energies. Therefore it is reasonable to assume that both spacer widths are equal. The results discussed here and those from the other specimens are listed in Tables I and II; they contain the corrected spacer widths obtained from SIMS. It should be mentioned that SIMS measurements give up to 25% variation on different specimens of the same epitaxy. This can be partly attributed to SIMS resolution (15%) and partly to doping variation along the sample.

Figure 2(c) shows a self-consistent calculated valence-band diagram for 300 K which will be discussed below.

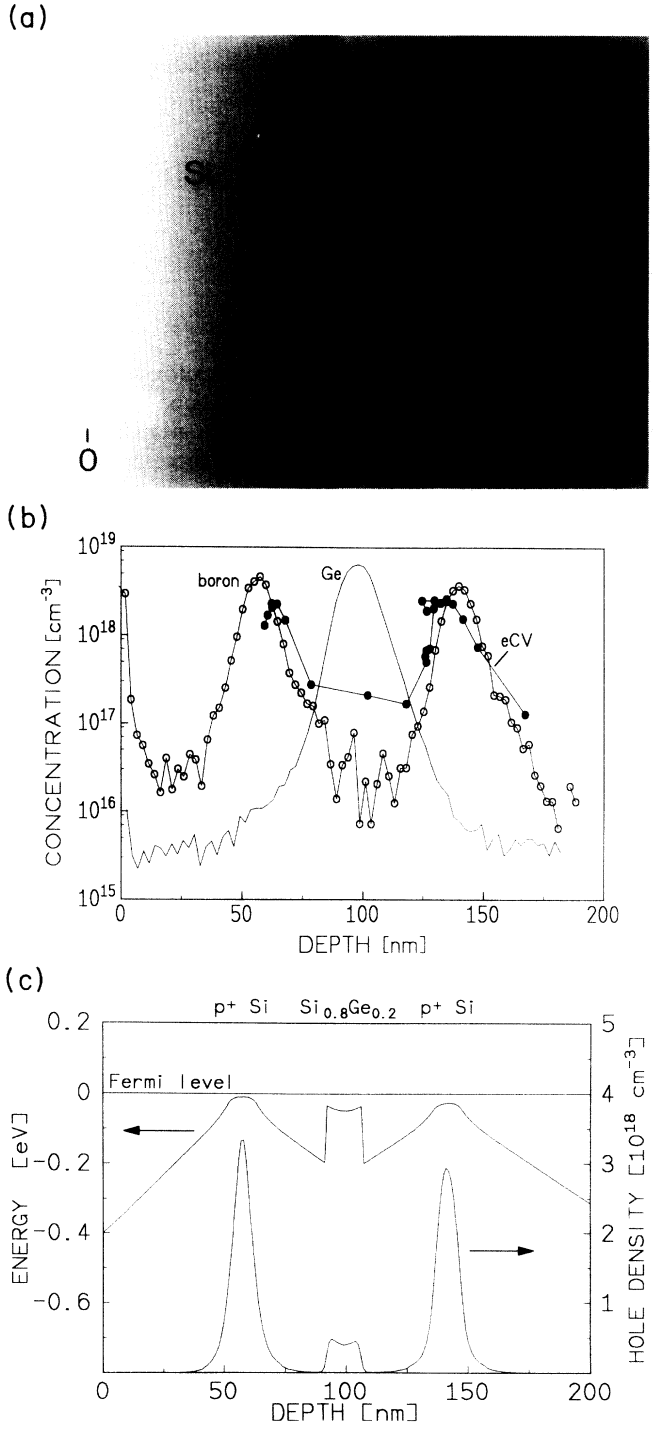

FIG. 2. Modulation-doped sample 534. (a) TEM image, (b) SIMS profile of boron and germanium and eCV profile of the free holes, and (c) self-consistently calculated valence-band diagram and hole distribution at 300 K.

IV. EFFECTIVE MASS OF HOLES OF STRAINED $Si_{1-x}Ge_x$ AND VALENCE-BAND DIAGRAM

$Si_{1-x}Ge_x$ has a larger bulk lattice constant than Si, and therefore, when grown strained on Si, significant changes in the band structure are produced.[25] The main changes are the reduction of the band gap in the $Si_{1-x}Ge_x$ layer as compared to unstrained $Si_{1-x}Ge_x$ and the lifting of the degeneracies of the valence and conduction bands in the layer.[26,27] In fact, the strain leads to a splitting of the heavy- and the light-hole bands, the heavy-hole band being shifted upwards, and the light-hole band being shifted downwards.[25] In strained $Si_{1-x}Ge_x$ layers the effective masses are changed too, in comparison to unstrained $Si_{1-x}Ge_x$ layers. The effective masses of strained $Si_{1-x}Ge_x$ films grown on a Si substrate along the [001] growth direction were calculated by solving the 6×6 Luttinger-Kohn Hamiltonian with consideration of the interaction of the spin-orbit band with the heavy- (HH) and light-hole (LH) bands. The results of our calculations are plotted for the [100] direction in Fig. 3(a) and for the [001] direction in Fig. 3(b) and agree with published data.[28] As expected, the effective hole mass depends on the Ge concentration and is different for different directions. It must be mentioned that the transverse [100] heavy-hole mass becomes smaller than the light-hole mass for $x>0$. This discontinuous behavior can be explained by the fact that in strained $Si_{1-x}Ge_x$ the strain-induced energy splitting between the two states immediately overwhelms the $\mathbf{k}\cdot\mathbf{p}$ coupling (which is arbitrarily small as $\mathbf{k}$ goes to zero).

For the calculation of the valence-band edge (see below) the values of interest are for $x=0.20$ $m^*_{HH}[100]=0.19m_0$ and $m^*_{HH}[001]=0.27m_0$. These values are lower than the effective hole masses in intrinsic bulk Si [$m^*_{HH}(001)=0.29m_0$] and therefore the lattice-limited mobility in a modulation-doped $Si/Si_{1-x}Ge_x$ heterostructure with a 2DHG in the $Si_{1-x}Ge_x$ channel should be higher than in bulk Si.

With these values for the effective masses and the acceptor concentration from the SIMS measurement, the valence-band diagram and hole density were calculated by self-consistently solving the Schrödinger and Poisson equations in the Hartree approximation [Figs. 2(c) and 4]. The valence-band edge was obtained by requiring that the Fermi level E_F remains constant throughout the structure. A surface potential pinning of 0.4 eV above the valence-band edge[29] and a valence-band offset ΔE_V of 0.185 eV (Ref. 30) at the $Si/Si_{0.8}Ge_{0.2}$ interfaces were assumed.

The result of the calculation at 300 K is shown in Fig. 2(c). One can see that only a small fraction of the holes

TABLE II. Experimental results of the samples listed in Table I. The three-dimensional acceptor and hole concentrations from the samples with two thin boron layers are peak values and the depth of the boron-doped layer represents the position of these peak values. The two-dimensional SIMS and eCV data of these samples give the densities of each doping layer, whereas the two-dimensional Hall data of these samples give the densities of both doped layers at 300 K. The other specimens are homogeneously doped layers and the depth of the boron-doped layer represents the thickness of the epitaxially grown layer. Hall samples were 8×8 mm^2. Samples marked with * have contacts on the periphery. For all the other samples the contacts were ~0.5 mm inside the sample.

Sample no.	Boron conc. 10^{18} cm^{-3} SIMS	Hole conc. 10^{18} cm^{-3} eCV	Hole conc. 10^{18} cm^{-3} Hall	Depth of the boron-doped layer (nm) SIMS	Depth of the boron-doped layer (nm) eCV	Sheet B conc. 10^{12} cm^{-2} SIMS	2D hole conc. 10^{12} cm^{-2} eCV	2D hole conc. 10^{12} cm^{-2} Hall	Hole mobility (cm^2/V s)
459	1.1±0.2	1.0±0.5	0.6±0.03	110±11	133±13				300 K: 203±10
436	2.7±0.5	2.1±0.3	2.2±0.1	141±14	126±13				300 K: 87±4
437	3.6±0.7	3.3±0.5	4.3±0.2	138±14	109±10				300 K: 79±4
438	8.7±1.7	6±2	7.4±0.4	200±20	239±24				300 K: 58±3
476	5.1±1.0	3.5±0.4		42±4	55±6	5.5±1.0			
	5.2±1.0	1.3±0.1		80±8	88±9	4.9±1.0	2.0±0.2	300 K: 11±5	300 K: 68±4
475	1.0±0.2	1.3±0.5	0.79±0.04					300 K: 16±1	300 K: 101±10
								4.2 K: 3.3±0.3	4.2 K: 470±47
479	3.4±0.7	0.64±0.10		26±3	62±9	3.5±0.7	1.0±0.2	300 K: 16±6	300 K: 42±20
	3.2±0.6	0.48±0.07		63±6	83±12	2.8±0.6	0.9±0.2	4.2 K: 1.6±0.1	4.2 K: 2400±120
478	3.7±0.7			30±3		3.9±0.8		300 K: 7.8±0.2	300 K: 86±5
	3.8±0.8	0.63±0.09		72±7	63±9	3.5±0.7	0.9±0.3	4.2 K: 1.6±0.1	4.2 K: 2800±140
509	2.9±0.6			32±3		4.0±0.8		300 K: 30±30	300 K: 20±15
	4.8±1.0			74±7		4.2±0.8		4.2 K:0.85±0.04	4.2 K: 1700±85
469	3.7±0.7			45±5		4.8±1.0		300 K: 11±3	300 K: 79±6
	4.0±0.8	1.8±0.3		102±10	105±16	4.7±0.9	3.0±0.6	4.2 K: 1.1±0.1	4.2 K: 3500±175
534	4.7±0.9	2.3±0.3		57±6	63±9	6.0±1.2	2.0±0.4	300 K: 16±1	300 K: 73±4
	3.7±0.7	2.3±0.3		140±14	134±20	4.9±1.0	4.7±0.9	4.2 K:0.54±0.03	4.2 K: 4600±230
534*	4.7±0.9	2.3±0.3		57±6	63±9	6.0±1.2	2.0±0.4	250 K: 13±1	250 K: 104±4
	3.7±0.9	2.3±0.3		140±14	134±20	4.9±1.0	4.7±0.9	4.2 K:0.40±0.02	4.2 K: 5900±300
535*	11±2.2	6.9±1.0		72±7	71±15	14±3	10±2	250 K: 25±1	250 K: 105±5
	9.2±1.8	6.7±1.0		173±17	158±24	13±3	14±3	4.2 K: 1.4±0.1	4.2 K: 2700±135

from the boron-doped Si layers moves into the $Si_{0.8}Ge_{0.2}$ layer. The calculated hole densities are (1) in the boron-doped layers $p=3.7\times10^{12}$ cm^{-2} (surface side) and $p=3.5\times10^{12}$ cm^{-2} (substrate side) and (2) only $p=6.2\times10^{11}$ cm^{-2} in the $Si_{0.8}Ge_{0.2}$ layer. Therefore we expect that room-temperature Hall-effect measurements yield primarily the electrical properties of the highly doped Si layers. According to these calculations, the wave function in the $Si_{0.8}Ge_{0.2}$ layer reaches from one $Si/Si_{0.8}Ge_{0.2}$ interface to the other, indicating that there is only one 2DHG in the $Si_{0.8}Ge_{0.2}$ layer instead of two at both $Si/Si_{0.8}Ge_{0.2}$ interfaces.

At 4 K (Fig. 4) the calculations show that the holes in the doped Si layers are frozen out and therefore only the holes in the $Si_{0.8}Ge_{0.2}$ layer are expected to contribute to the measured mobility. Furthermore, the calculations show that there is only one conducting channel (i.e., 2DHG) in the $Si_{0.8}Ge_{0.2}$ layer as for the 300-K case and only the first subband, which consist of heavy holes, is occupied. These properties were recognized in the SdH and QHE measurements as will be discussed in Sec. V. The calculated hole density in the $Si_{0.8}Ge_{0.2}$ layer at 4 K ($p=4.4\times10^{11}$ cm^{-2}) for this structure is almost the same as that at 300 K ($p=6.2\times10^{11}$ cm^{-2}).

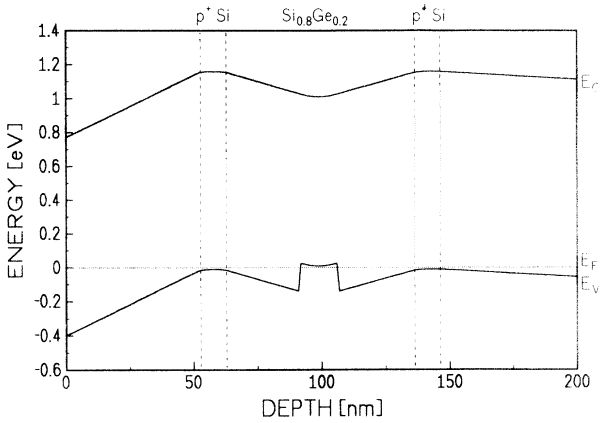

FIG. 4. Self-consistently calculated band edges of a modulation-doped $Si/Si_{0.8}Ge_{0.2}/Si$ structure at 4 K without illumination. The hole density in the QW was computed to be 4.4×10^{11} cm^{-2} (sample 534).

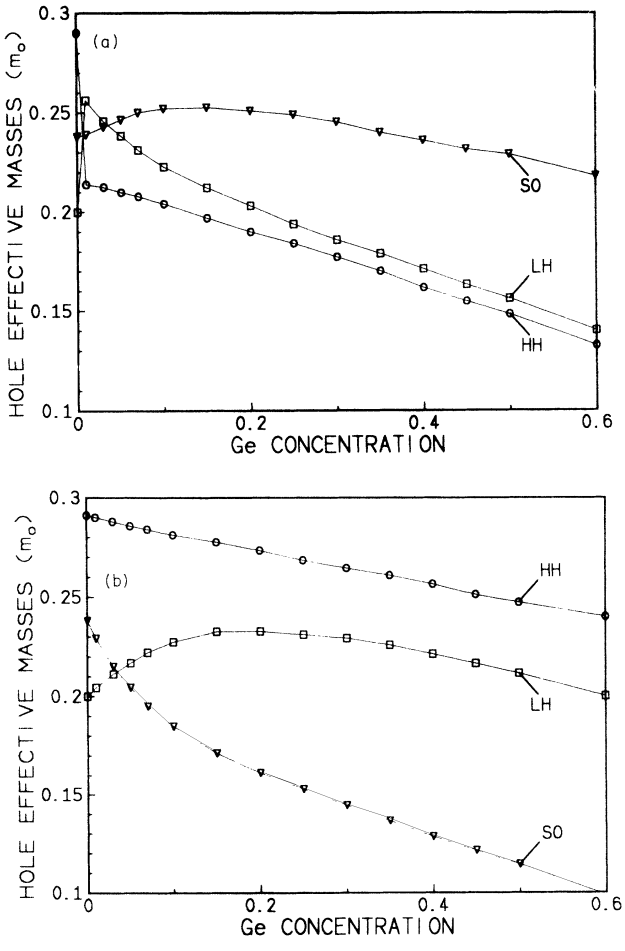

FIG. 3. Calculated effective hole mass at the Γ point for strained $Si_{1-x}Ge_x$ as a function of x (a) in the [100] direction and (b) in the [001] direction. In the [100] direction, the HH and LH masses are discontinuous at $x=0$. (In fact discontinuity occurs at strain = 0 due to degeneracy effects.)

V. MAGNETOTRANSPORT IN $Si/Si_{1-x}Ge_x/Si$ HETEROSTRUCTURES

A. Homogeneously doped Si layers

Prior to the growth of the modulation-doped samples, we made a calibration of the doping level at 300 K using eCV, Hall-effect, and SIMS measurements. For these measurements we used homogeneously doped Si layers (see Sec. II and Table I). Epitaxial growth conditions were a temperature of 700 °C, a total pressure of 0.12 torr. The doping gas was 20 ppm diborane in hydrogen. We used p-type (6 Ω cm) substrates for eCV and SIMS measurements and n-type (1000 Ω cm) substrates for Hall-effect and SIMS measurements. The results of these measurements are listed in Table II. The hole concentrations determined by eCV and Hall-effect measurements are, within the margin of error, in agreement with the SIMS measurements indicating that all boron atoms are electrically active at 300 K.

Figure 5 shows the boron concentration and hole concentration versus injection ratio [B]/[Si] in the gas phase. The efficiency of boron incorporation $(B/Si)_{solid}/(B/Si)_{gas}$ is approximately 11 (calculated from the SIMS measurements). This coefficient is related to the effective sticking coefficients of B_2H_6 and $SiCl_2H_2$. Comparing this value with the results of Meyerson *et al.*[31] (efficiency of boron incorporation ~3) and Dutartre *et al.*[32] (efficiency of boron incorporation ~6), we see that the boron incorporation is higher in our case. These differences might be due to the different growth conditions. Meyerson *et al.* used SiH_4 instead of $SiCl_2H_2$ in an UHV-CVD system (at 640 °C, $p\leq10^{-3}$ torr) while Dutartre *et al.* used SiH_4, too, but in a RTCVD system (at 610 °C, $p=0.26$ torr).

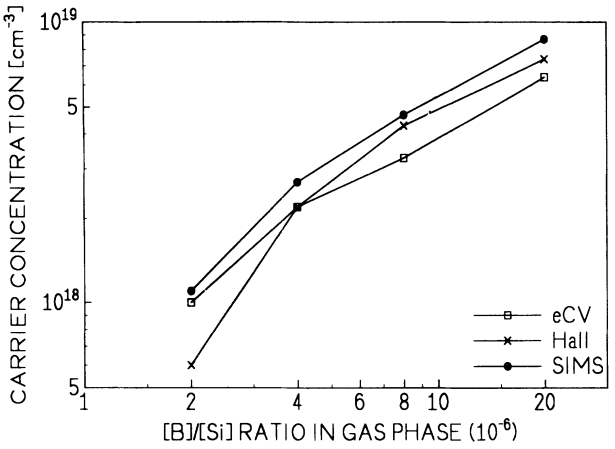

FIG. 5. Boron incorporation in Si versus injection ratio [B]/[Si] in the gas phase at 700 °C.

B. Si structure with two boron-doped layers

Furthermore, we have investigated a sample (sample 476) with two thin boron-doped layers. The doping concentration of the boron-doped layers (~ 10 nm thick) was as high as in the modulation-doped heterostructures ($\sim 5\times 10^{12}$ cm^{-2}). SIMS, eCV, and Hall-effect measurements yield results which are in reasonable agreement (Table II) showing that all boron atoms are fully activated. At this point we compared the sheet-hole concentrations of the eCV and Hall-effect measurements with the sheet-boron concentration of the SIMS measurement again. The holes freeze out at low temperatures (<70 K), justifying the latter assumption that there is negligible parallel conduction at low temperature in the doped Si layers in the modulation-doped heterostructures containing a 2DHG.

C. Homogeneously doped Si/$Si_{0.8}Ge_{0.2}$/Si heterostructure

Figure 6 shows the measured transport properties of a homogeneously doped Si/$Si_{0.8}Ge_{0.2}$/Si heterostructure (sample 475). At room temperature, the measured hole concentration is nearly equal to the hole concentration in the p^+ Si layers. By decreasing the temperature, holes in the p^+ Si layers are frozen out and below 50 K the hole concentration reaches a constant value indicating that a 2DHG is formed in the $Si_{0.8}Ge_{0.2}$ layer. The mobility at room temperature is $\mu_h = 101$ cm^2/V s, consistent with the expected mobility of a homogeneously doped Si layer at this doping level (1×10^{18} cm^{-3}) in which the mobility is limited by the scattering due to impurity atoms.[28] By decreasing the temperature the measured mobility increases as expected for structures containing a 2DHG because first phonon scattering is reduced and second the holes in the p^+ Si layers freeze out so that only the $Si_{0.8}Ge_{0.2}$ layer contributes to the hole transport. The hole mobility is now limited by scattering due to the background doping, which is very high (1×10^{18} cm^{-3}), and therefore the mobility of the 2DHG at 4.2 K is only 470 cm^2/V s.

D. Modulation-doped Si/$Si_{1-x}Ge_x$/Si heterostructures

The mobility can be increased further if the $Si_{1-x}Ge_x$ layer is not intentionally doped and is spatially separated from the p^+ Si layers by undoped spacers. This is the case for the modulation-doped heterostructures presented in Sec. III and Fig. 2. The temperature dependence of the hole concentration and hole mobility of the modulation-doped Si/$Si_{0.8}Ge_{0.2}$/Si heterostructure presented in Fig. 2 (sample 534) is shown in Fig. 6. Self-consistent calculations at 300 K (see Sec. IV) have shown that only a small part of the holes moves into the $Si_{0.8}Ge_{0.2}$ layer and this concentration does not significantly change with temperature. Therefore at 300 K the measured mobility and hole concentration are dominated by the values of the p^+ Si regions. The hole mobility at 300 K of the modulation-doped structures is lower than the measured hole mobility of the homogeneously doped $Si_{0.8}Ge_{0.2}$/Si sample 475, because the p^+ layers in the modulation-doped heterostructures contain a higher boron concentration. The measured mobility at 300 K ($\mu_h \sim 73$ cm^2/V s) is nearly the same as the mobili-

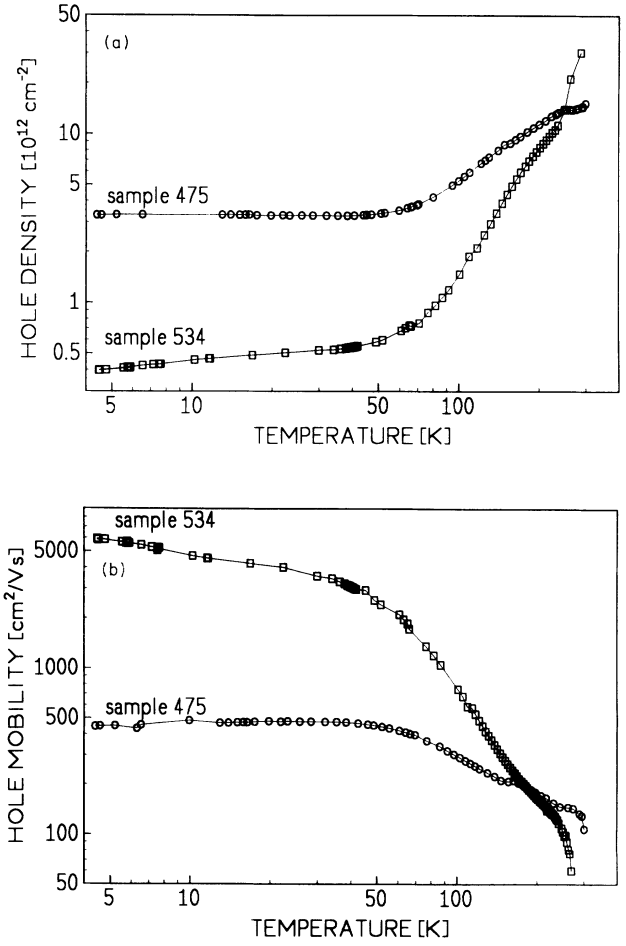

FIG. 6. Temperature dependence for a modulation-doped (sample 534) and a homogeneously doped (sample 475) Si/$Si_{0.8}Ge_{0.2}$/Si structure of (a) Hall concentration and (b) Hall mobility.

ty of the Si structure with two p^+ layers (sample 476, $\mu_h \sim 68$ cm^2/V s). One can conclude that the contribution of the holes in the p^+ Si was much higher than that of the holes in the $Si_{1-x}Ge_x$ channel, but it was not possible to extract a value for $\mu_{Si_{0.8}Ge_{0.2}}$.

Several authors have discussed the 300-K hole mobility in $Si_{1-x}Ge_x$.[28,33–35] Manku and Nathan[34] calculated the hole mobility of strained intrinsic $Si_{1-x}Ge_x$ using an expression derived from a first-order perturbation solution of the Boltzmann transport equation. Using a value of 0.27 eV for the alloy interaction potential they get an in-plane mobility of $\mu_h \approx 500$ cm^2/V s for $Si_{0.8}Ge_{0.2}$ layers. Chun and Wang[28] also used the relaxation-time approximation while Hinckley and Singh[35] used a Monte Carlo simulation to calculate the hole mobility of intrinsic strained $Si_{1-x}Ge_x$ layers. These two groups have used a value of 0.20 eV for the alloy interaction potential. Due to the lower value of the alloy interaction potential, they obtained a higher value for the in-plane hole mobility at 300 K (1135 and 1300 cm^2/V s, respectively) than Manku and Nathan.[34]

Chun and Wang also calculated mobilities at 300 K for doped $Si_{1-x}Ge_x$ layers but neglecting quantum effects. Laikhtman and Kiehl[33] have included quantum effects in the calculations of the hole mobility in $Si/Si_{0.6}Ge_{0.4}/Si$ heterostructures. Nevertheless, it is clear that, due to the lower hole effective mass in strained $Si_{1-x}Ge_x$ layers, it should be possible to reach higher hole mobilities in modulation-doped heterostructures at room temperature. Therefore investigations have to be concentrated on the improvement of the hole mobility at 300 K.

The temperature dependence of the measured hole mobility of the modulation-doped sample 534 is shown in Fig. 6. Lowering the temperature, starting from 300 K, holes in the p^+ regions are frozen out and the holes in the $Si_{0.8}Ge_{0.2}$ layer become noticeable; the measured mobility (which is determined by contributions from three layers, two p^+ Si layers and the strained $Si_{0.8}Ge_{0.2}$ layer), increases. At temperatures below 30 K the measured mobility reflects only the nature of the 2DHG because the holes in the p^+ Si layers which are not transferred into the $Si_{0.8}Ge_{0.2}$ channel are frozen out. Below 30 K we observe only a weak temperature dependence of hole mobility and concentration which demonstrates the presence of a 2DHG confirmed by SdH and QHE measurements (see below). The measured hole concentration at 4.2 K ($p = 4.0 \times 10^{11}$ cm^{-2}) agrees well with the self-consistent calculations at 4 K ($p = 4.4 \times 10^{11}$ cm^{-2}). The measured mobility at this temperature is $\mu_h = 5900$ cm^2/V s. The rather lower 2D hole mobility at low temperatures can be attributed to the fact that the mobility is limited by alloy scattering.[8] In Ref. 8 the alloy scattering mobility μ_{alloy} was calculated using the expression

$$\mu_{\text{alloy}} = 16e\hbar^3\{3b(m_\parallel)^2 x(1-x)U^2\Omega\}^{-1},$$

where Ω is the volume of the unit cell, $b = \{4e^2 m_v p/\hbar^2\varepsilon\}$ is the inverse spatial extension of the Fang and Howard wave function, m_v the effective mass in the direction of quantum-well confinement, $m_\parallel$ the in-plane hole mass of $Si_{1-x}Ge_x$, U the alloy interacting potential, x the Ge composition in the $Si_{1-x}Ge_x$ layer, and ε the dielectric constant. With $U = 0.5$ eV and a hole density $p = 2 \times 10^{11}$ cm^{-2}, they get $\mu_{\text{alloy}} \sim 5000$ cm^2/V s.[8] Because the alloy scattering rate varies with U^{-2}, smaller values of U will yield larger mobilities. In Refs. 28, 34, and 35 lower values for U are assumed (see above) but, to our knowledge, no calculation for the alloy interacting potential is available for a more exact prediction of the mobility due to alloy scattering.

Figure 7 shows the dependence on spacer thickness of the hole concentration [Fig. 7(a)] and hole mobility [Fig. 7(b)] for $T = 4.2$ and 77 K. In these samples the Ohmic contacts were ~ 0.5 mm inside the sample and therefore the measurement accuracy was only 25%. The Ohmic contacts of the modulation-doped specimen discussed above and plotted in Fig. 6 (sample 534) lie at the edge of the specimen. In those measurements the van der Pauw condition is fulfilled and the results are more reliable. Figure 7(b) shows that at low temperatures (4.2 K) the mobility rises with increasing spacer thickness. This is an

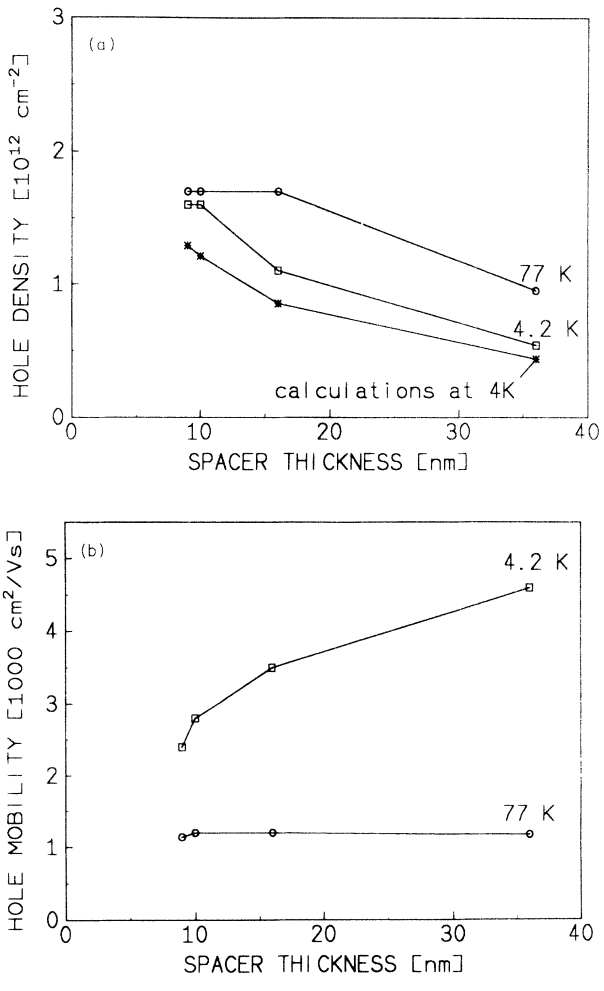

FIG. 7. Spacer dependence for modulation-doped $Si/Si_{0.8}Ge_{0.2}/Si$ structures. (a) Hall concentration measured at 4.2 and 77 K and calculated at 4 K and (b) Hall mobility measured at 4.2 and 77 K.

indication that the mobility is limited by scattering on remote ions and/or boron diffused into the $Si_{0.8}Ge_{0.2}$ channel.

At 77 K the mobility is nearly independent of spacer thickness [Fig. 7(b)]. This can be explained by the fact that at higher temperatures the mobility of the 2DHG is limited by phonon scattering, which is independent of the spacer thickness. Moreover, not all holes in the boron-doped layers are frozen out and therefore contribute to the measured mobility. The mobility of the p^+ Si layers ($\sim 5\times10^{18}$ cm^{-3}) is limited by impurity scattering. Since the doping level of all modulation-doped heterostructures is the same, the mobility of the holes in these boron-doped layers is nearly equal. In Fig. 7(a) the measured and calculated hole concentrations are plotted, showing reasonable agreement at low temperatures. As expected, the hole concentration in the QW region decreases with spacer thickness. The measured hole concentration at 77 K is somewhat higher than at 4.2 K, due to the contribution of holes in the p^+ Si layers at 77 K.

Figure 8 shows well-defined SdH oscillations and clear QHE plateaus of the sample with the highest Hall mobility at 4.2 K (5900 cm^2/V s). The onset of SdH oscillations is already observable at fields as low as $B=0.5$ T. Apart from filling factor $\nu=2$ and 4, only odd filling factors were observed. This is possibly due to the overlap of Landau levels because of the low spin splitting at lower fields.[3,6] The low-field Hall-effect hole density at 50 mK was $p_{\rm Hall}=4.5\times10^{11}$ cm^{-2} while the density determined from SdH measurements was $p_{\rm SdH}=4.8\times10^{11}$ cm^{-2}. The fact that $p_{\rm Hall}\approx p_{\rm SdH}$ indicates that only one 2D conducting channel (i.e., only one 2DHG) is present in the $Si_{0.8}Ge_{0.2}$ layer, in agreement with the self-consistent calculations shown in Figs. 2(c) and 4. If two 2DHG's were present, the measured Hall-effect concentration should be two times higher than the hole concentration obtained by SdH measurements. Furthermore, at low magnetic fields, where the spin splitting is not resolved, we would find filling factors only with $\nu=4n+1$ instead of $\nu=2n+1$, where n is an integer in that case. But in our specimen at low magnetic fields, only two Landau levels are crossing the Fermi level instead of four, indicating that only one conducting channel (i.e., only one 2DHG) is present. The longitudinal resistivity R_{xx} vanishes at filling factors smaller than 4, indicating that there are no parallel conducting channels to the 2DHG. Another feature is that no harmonic components in the oscillation spectrum of R_{xx} are observed, which is an indication that only the first subband in the $Si_{0.8}Ge_{0.2}$ layer is occupied. From the SdH oscillations we derive a mobility of 6460 cm^2/V s at 50 mK in agreement with the Hall-effect measurement at 50 mK (6870 cm^2/V s). These values are comparable with the best results published so far for $x\sim0.2$.[3,5,6,9,10]

VI. PHOTOLUMINESCENCE OF 2DHG IN $Si/Si_{1-x}Ge_x/Si$

PL spectra of a modulation-doped sample (sample 535) are presented in Fig. 9. The no-phonon transitions and their TO-phonon replicas arising from the $Si_{0.8}Ge_{0.2}$ QW are observed similarly as reported by many other authors for undoped structures.[30,36–40] By temperature- and excitation-power-density-dependent measurements the different no-phonon peaks were assigned to localized excitons (LE's), bound excitons (BE's), and free excitons (FE's). In Fig. 9 PL spectra for three different excitation power densities (P) are shown. The intensity $I\sim P^m$ of the FE peak exhibits a linear to superlinear behavior with $m=1-1.3$ while the BE peak varies sublinearly with $m=0.79-0.94$. The LE peak shows saturation behavior typical for localized excitons.[37] The FE and BE peaks are very sharp with full widths at half maximum of 4–6 meV. With increasing temperature only the FE peak remains. The energy difference between the FE and the BE peaks (~5 meV) is the typical binding energy for excitons bound to shallow impurities, which are very probably residual boron ($\sim1\times10^{16}$ cm^{-3}). The energy shift with excitation-power density of the FE peak is, as expected, small, being of the order of 2 meV.

Therefore, there is no marked difference to undoped samples except that the PL intensity is enhanced by more than one order of magnitude. Figure 10 shows the corre-

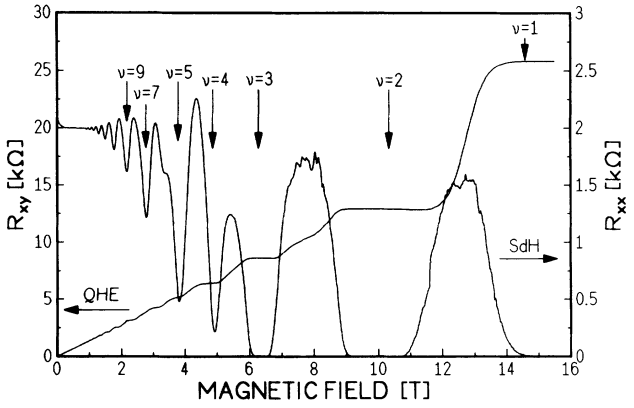

FIG. 8. Results of QHE and SdH measurements at 50 mK of the modulation-doped sample with the highest mobility (sample 534).

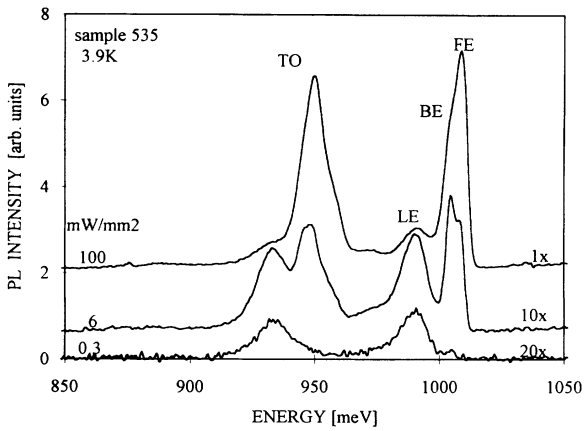

FIG. 9. PL spectra of a modulation-doped sample (sample 535) at different excitation power densities at 4.2 K.

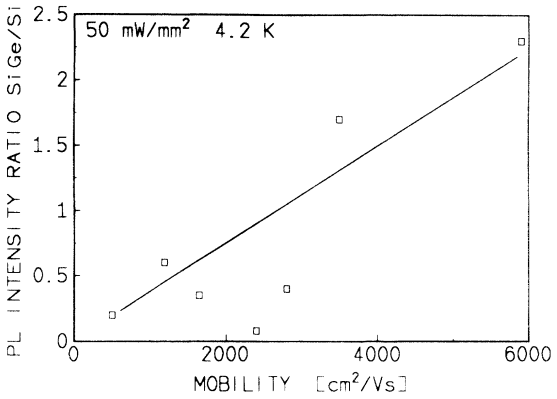

FIG. 10. Correlation between PL intensity and mobility of the modulation-doped samples. The PL intensity ratio is given by the ratio of free-exciton peak heights of $Si_{1-x}Ge_x$ and Si at 4.2 K.

lation of the PL signal with the mobility of the modulation-doped samples. An explanation of the enhancement of PL intensity with increasing mobility might be the existence of an attractive potential in the conduction band (see Fig. 4). The well in the conduction band is the result of modulation doping causing a confinement of the photoexcited electrons in the region of the $Si_{0.8}Ge_{0.2}$ layer.

VII. CONCLUSIONS

In conclusion, we have observed high mobility and intense photoluminescence of LPCVD-grown modulation-doped $Si/Si_{1-x}Ge_x/Si$ heterostructures. This demonstrates the high quality of the $Si/Si_{1-x}Ge_x$ heterointerfaces and the low concentration of impurities and defects; it also indicates that LPCVD is a suitable method for the fabrication of structures containing 2DHG's with mobilities comparable to the best published values. We have performed effective-mass and self-consistent valence-band calculations. The predictions made in these calculations are confirmed in Hall, SdH, and QHE measurements.

It was shown that *p*-type modulation doping causes a strong enhancement of luminescence compared to undoped samples. This might be explained by the additional confinement of the photoexcited electrons by an attractive potential caused by the modulation doping.

ACKNOWLEDGMENTS

The authors wish to thank G. Abstreiter for interesting discussions, A. Souifi for the critical reading of the manuscript, and K. Wambach for technical assistance.

[1]F. Schäffler, in *Silicon Molecular Beam Epitaxy,* edited by J. C. Bean, S. Iyer, and K. Wang, MRS Symposia Proceedings No. 220 (Materials Research Society, Pittsburgh, 1991), p. 433.

[2]R. People, J. C. Bean, and D. V. Lang, J. Vac. Sci. Technol. A **3**, 846 (1985).

[3]J. F. Nützel, F. Meier, E. Friess, and G. Abstreiter, Thin Solid Films **222**, 150 (1992).

[4]D. W. Smith, C. J. Emeleus, R. A. Kubiak, E. H. C. Parker, and T. E. Whall, Appl. Phys. Lett. **61**, 1453 (1992).

[5]T. Mishima, C. W. Fredrikz, G. F. A. van de Walle, D.J. Gravenstijn, R. A. van den Heuvel, and A. A. van Gorkum, Appl. Phys. Lett. **57**, 2567 (1990).

[6]F. F. Fang, P. J. Wang, B. S. Meyerson, J. J. Nocera, and K. E. Ismail, Surf. Sci. **263**, 175 (1992).

[7]V. Venkataraman, P. V. Schwartz, and J. C. Sturm, Appl. Phys. Lett. **59**, 2871 (1991).

[8]Y. Guldner, J. M. Berroir, J. P. Vieren, M. Voos, I. Sagnes, P. A. Badoz, P. Warren, and D. Dutartre, Phys. Rev. B **48**, 12 312 (1993).

[9]L. Vescan, R. Loo, A. Hartmann, U. Zastrow, A. Leuther, T. Schäpers, T. Stoica, and H. Lüth, in *Proceedings of the Fourth International Conference on the Formation of Semiconductor Interfaces, Jülich, Germany,* edited by B. Lengeler, H. Lüth, W. Mönch, and J. Pollman (World Scientific, New York, 1994), pp. 597–600.

[10]R. Apetz, R. Loo, L. Vescan, A. Hartmann, U. Zastrow, A. Leuther, T. Schäpers, and H. Lüth, Solid-State Electron. **37**, 957 (1994).

[11]D. K. Nayak, J. C. S. Woo, J. S. Park, K.-L. Wang, and K. P. MacWilliams, IEEE Electron Device Lett. **12**, 154 (1991).

[12]V. P. Kesan, S. Subbanna, P. J. Restle, M. J. Tejwani, J. M. Altken, S. S. Iyler, and J. A. Ott, IEEE Int. Electron Device Meeting **8–11**, 25 (1991).

[13]P. M. Garone, V. Venkataraman, and J. C. Sturm, IEEE Electron Device Lett. **13**, 56 (1992).

[14]S. Verdonckt-Vandebroek, E. F. Crabbé, B. S. Meyerson, D. L. Harame, P. J. Restle, J. M. C. Stork, A. C. Megdanis, C. L. Stanis, A. A. Bright, G. M. W. Kroesen, and A. C. Warren, IEEE Electron Device Lett. **12**, 447 (1991).

[15]T. P. Pearsall and J. C. Bean, IEEE Electron Device Lett. **7**, 308 (1986).

[16]H. P. Tang, L. Vescan, and H. Lüth, J. Cryst. Growth **116**, 1 (1992).

[17]L. Vescan, W. Jäger, C. Dieker, K. Schmidt, A. Hartmann, and H. Lüth, in *Mechanisms of Heteroepitaxial Growth,* edited by M. F. Chisholm, R. Hull, L. J. Schowalter, and B. J. Garrison, MRS Symposia Proceedings No. 263 (Materials Research Society, Pittsburgh, 1992), p. 23.

[18]U. Zastrow, L. Vescan, R. Butz, K. Schmidt, and C. Dieker, in *Secondary Ion Mass Spectrometry SIMS IX,* edited by Alfred Benninghoren (Wiley, New York, 1994).

[19]P. Blood, Semicond. Sci. Technol. **1**, 7 (1986).

[20]Phan Minh Tan, Phys. Status Solidi A **37**, 439 (1976).

[21]R. Sauer, J. Weber, J. Stolz, E. R. Weber, K.H. Küsters, and H. Alexander, Appl. Phys. A **36**, 1 (1985).

[22]E. F. Schubert, J. M. Kuo, and R. F. Kopf, J. Electron. Mater. **19**, 521 (1990).

[23]A. A. van Gorkum and K. Yamaguchi, IEEE Trans. Electron Devices **ED-36**, 410 (1989).

[24]K. Lehovic, Solid State Electron. **27**, 1097 (1984).

[25]T. Manku and A. Nathan, Phys. Rev. B **43**, 12 634 (1991).

[26]R. People, IEEE J. Quantum Electron. **QE-22**, 1696 (1986).

[27]S. S. Iyler, G. L. Patton, J. M. C. Stork, B. S. Meyerson, and D. L. Harame, IEEE Trans. Electron Devices **ED-36**, 2043 (1989).

[28]S. K. Chun and K. L. Wang, IEEE Trans. Electron Devices **ED-39**, 2153 (1992).

[29]L. Ley, M. Cardona, and R. Pollak, in *Photoemission in Solids II,* edited by L. Ley and M. Cardona, Topics in Applied Physics Vol. 27 (Springer-Verlag, Berlin, 1979), Chap. 2, pp. 11–172.

[30]D. Dutartre, G. Bremond, A. Souifi, and T. Benyattou, Phys. Rev. B **44**, 11 525 (1991).

[31]B. S. Meyerson, F. K. Legoues, T. N. Nguyen, and D. L. Harame, Appl. Phys. Lett. **50**, 113 (1987).

[32]D. Dutartre, P. Warren, I. Sagnes, P. A. Badoz, A. Perio, J. C. Dupuis, and G. Prudon, J. Vac. Sci. Technol. B **11**, 1134 (1993).

[33]B. Laikhtman and R. A. Kiehl, Phys. Rev. B **47**, 10 515 (1993).

[34]T. Manku and A. Nathan, IEEE Electron Device Lett. **12**, 704 (1991).

[35]J. M. Hinckley and J. Singh, Phys. Rev. B **41**, 2912 (1990).

[36]J. C. Sturm, H. Manoharan, L. C. Lenchyshyn, M. L. W. Thewalt, N. L. Rowell, J.-P. Noël, and D. C. Houghton, Phys. Rev. Lett. **66**, 1362 (1991).

[37]L. C. Lenchyshyn, M. L. W. Thewalt, J. C. Sturm, P. V. Schwartz, E. J. Prinz, N. L. Rowell, J.-P. Noël, and D. C. Houghton, Appl. Phys. Lett. **60**, 3174 (1992).

[38]L. Vescan, A. Hartmann, K. Schmidt, Ch. Dieker, and H. Lüth, Appl. Phys. Lett. **60**, 2183 (1992).

[39]J. Brunner, U. Menczigar, M. Gail, E. Friess, and G. Abstreiter, Thin Solid Films **222**, 27 (1992).

[40]S. Fukatsu, H. Yoshida, N. Usami, A. Fujiwara, Y. Takahashi, Y. Shiraki, and R. Ito, Thin Solid Films **222**, 1 (1992).

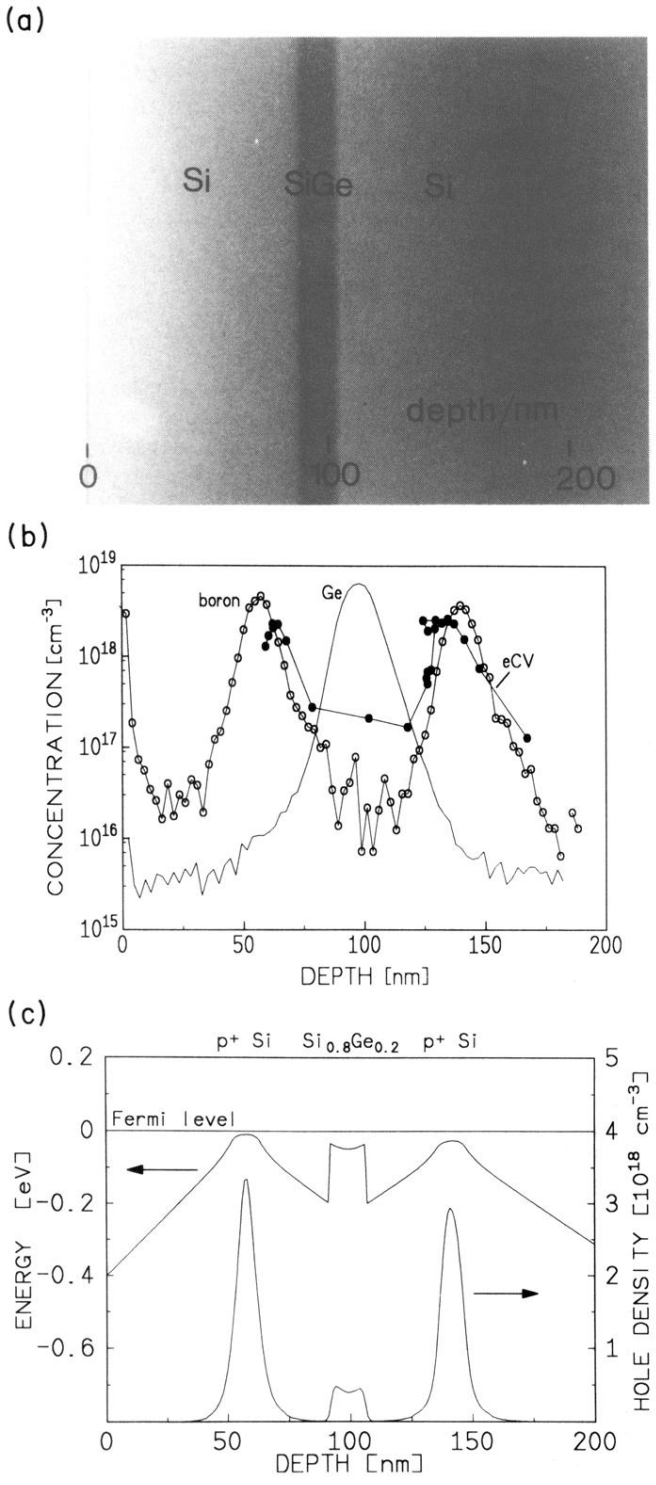

FIG. 2. Modulation-doped sample 534. (a) TEM image, (b) SIMS profile of boron and germanium and eCV profile of the free holes, and (c) self-consistently calculated valence-band diagram and hole distribution at 300 K.